IEEE Access
Multidisciplinary | Rapid Review | Open Access Journal

Date of publication xxxx 00, 0000, date of current version xxxx 00, 0000.

Digital Object Identifier —

A 10-Ports MIMO Antenna System for 5G Smart-Phone Applications

RIZWAN ULLAH[1], SADIQ ULLAH[*1], (SENIOR MEMBER, IEEE), RAZA ULLAH[1], FAROOQ FAISAL[2], ISMAIL BEN MABROUK[3,4], (SENIOR MEMBER, IEEE), MUATH JODEI AL HASAN[3], (SENIOR MEMBER, IEEE)

[1]Telecommunication Engineering Department, University of Engineering & Technology, Mardan, KPK, Pakistan
[2]Department of Electrical Engineering, University of Quebec, Val d'Or, Canada
[3]Department of Electrical Engineering, Al Ain University of Science and Technology, Abu Dhabi 64141, UAE
[4]Durham University, Engineering Department, UK

Corresponding author: Sadiq Ullah (e-mail: sadiqullah@uetmardan.edu.pk).

The publication of this article was funded by the Abu-Dhabi Department of Education and Knowledge (ADEK) Award for Research Excellence, in 2019, under Grant AARE19-245.

ABSTRACT This paper presents a 10-ports, hybrid multiple-input multiple-output (MIMO) antenna system for 5G Smartphone applications. The proposed antenna system comprises two types of antenna modules: (1) multi-band module consists of two identical multiband antenna elements, each antenna element in this module covers the 2G bands (GSM 850/900/1800/1900 MHz), 3G band (UMTS 2100 MHz) and 4G bands (LTE 2300/2500), and (2) single-band module consists of eight identical L shape elements, each antenna element in this module covers the C-band (3400-3600 MHz) for 5G mobile application. The overall dimensions of the proposed antenna system are $150 \times 80\ mm^2$. The proposed antenna system is fabricated and tested. Experimental results show reflection coefficients better than -6 dB and -10 dB for multi-band and single-band modules, respectively, with high isolation levels between the antenna elements in both modules. Moreover, the measured envelop correlation coefficients (ECC) is well below 0.3 and 0.1 for the proposed multi-band and single-bands modules, respectively. In addition, single antenna elements in both modules show good radiation characteristics with maximum peak gain between 2 dBi and 4 dBi. Finally, 43 bps/Hz channel capacity is achieved in the single-band module. With these characteristics, the proposed antenna system can be a good candidate in the modern mobile communication systems.

INDEX TERMS 5G, MIMO, ECC, mobile communication.

I. INTRODUCTION

With the rapid advancements in the mobile communication technology, mobile communication networks have become heterogeneous kind of network environment, which can support multiple frequency bands of different cellular generations [1]. The first generation (1G) was introduced for supporting analogue voice calls service. Later on, the second generation (2G) introduced new features like short message service (SMS) and digital voice calls. After that, the third generation (3G) was introduced with multimedia services such as high-speed internet, high quality video and voice calls services. Finally, very high-speed internet services over severe multipath channel environments was introduce in the fourth generation (4G) [2].

The fifth generation (5G) mobile communications have now become available. 5G provides higher capacity, massive connectivity, low latency, and higher reliability over multi-path environment [3]–[5]. In order to achieve these goals MIMO technology has become one of promising technology. Currently, 2×2 MIMO antenna system has been efficiently used in 4G mobile communication [6]. As reported in [7], expected data rates for 5G will be 100 times more than the currently used 4G technology, and hence this data rate cannot be achieved by using the conventional 2×2 or even 4×4 MIMO antenna systems. To achieve the desired data rate, at least six to eight antenna elements should be integrated in a single 5G mobile handset [7]. Currently, several countries and regions have already started testing and defining standard for future 5G mobile communication. In Nov 2015, world radio communication conference (WRC 2015) have agreed to allocate C-band (3400-3600 MHz) [8] for 5G mobile communication. China has also started work on the same C-

This article has been accepted for publication in a future issue of this journal, but has not been fully edited. Content may change prior to final publication. Citation information: DOI 10.1109/ACCESS.2020.3042750, IEEE Access

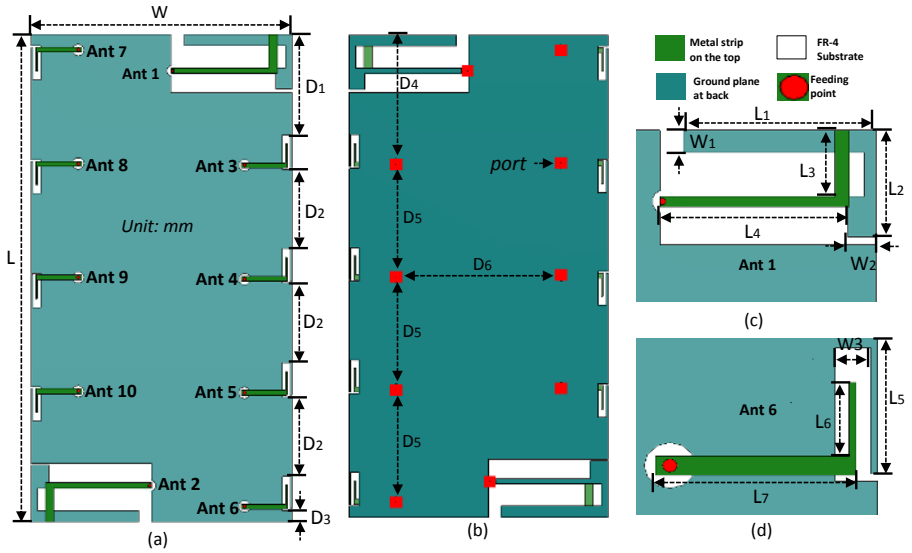

FIGURE 1: Geometry and detail physical dimensions of the proposed MIMO antenna system (Units: mm): (a) Front View. (b) Back view. (c) Zoom view of the unit multi-band antenna element (Ant-1). (d) Zoom view of the unit single-band antenna element (Ant-6).

Dimensions	value	Dimensions	vale	Dimensions	value
L	150 mm	W	80 mm	D1	31 mm
D2	24.5 mm	D3	3.5 mm	D4	40.5 mm
D5	35.5 mm	D6	46.0 mm	L1	31.4 mm
W1	3.50 mm	L2	17.5 mm	W2	3.0 mm
L3	10.40 mm	L4	32.5 mm	W3	2.5 mm
L5	10.50 mm	L6	5.8 mm	L6	14 mm

TABLE 1: Detailed physical dimensions of the proposed MIMO antenna system.

Country	<1 GHz	3 GHz	4 GHz	5 GHz	24-28 GHz	37-42 GHz
United states	600 MHz	3.4-3.6 GHz	-	5.9-7 GHz	27.4-28.4 GHz	37-37.8
China	-	3.3-3.6 GHz	-	-	24-27 GHz	-
Uk	-	3.4-3.8 GHz	-	-	26, 28 GHz	-
Canada	-	3.4-3.6 GHz	-	5.9-7 GHz	27.4-28.4 GHz	37.6-40 GHz
Australia	-	3.4-3.7 GHz	4.4-5 GHz	-	28 GHz	39 GHz
EU	700 MHz	3.4-3.8 GHz	-	5.9-6.5 GHz	24-27 GHz	-

TABLE 2: The details of the world wide spectrum for 5G.

band, while European Union and Korea have selected 3400-3800 MHz and 3400-3700 MHz, respectively, for 5G mobile communication [9], [10]. Table 2 summarizes the world wide spectrum for 5G communication [11].

Recently, a number of MIMO antenna systems have been investigated for mobile phone application. Initially the MIMO system were proposed for WiMAX, WLAN and LTE bands, such as: a dual elements MIMO system operating at 3.6 GHz for WiMAX applications [12], 2.5-2.7 GHz band for LTE [13], and 5 GHz for WLAN band [14]. Multi-band MIMO antenna systems have also been reported in literature like dual-band 2.4/5 GHz band for WLAN [15], 2.1/2.4 GHz for UMTS and WLAN [16], and 2.1/2.6 GHz for UMTS and LTE applications [17]. In [18], a tri-band MIMO antenna system covering the frequency ranges of 2.07-2.52 GHz, 4.28-4.50 GHz, and 5.67-7.27 GHz was reported.

Similarly, several other MIMO antenna systems have been reported in the literature for the 5G smartphone applications [19]–[30]. These systems demonstrate its superiority in terms of isolation, ECC, and channel capacity. To improve the isolation between the antenna elements, different techniques such as spatial diversity in [19] and polarization diversity in [20], [21], using neurulation line between the antenna elements [22], and slotted ground plane to stop the propagation of the signal from one port to another port in [23]–[25], have been proposed. Two different approaches have been adopted in the literature for achieving high channel capacity. In the first approach, the impedance bandwidth was improved to involve different frequency spectrum [26]–[28], while, in the second approach, higher order MIMO system (increasing the number of antenna elements) were used [29]–[31]. Even though, a large number of MIMO antenna systems have been reported and investigated in literature for the 5G smartphone applications, which shows good results in the desired frequency bands. However, to the best of our knowledge, they did not investigate a suitable MIMO system that could cover the frequency bands of all generation including 2G, 3G, 4G, and 5G.

In this study, a 10-ports MIMO antenna system is proposed for the 5G Mobile applications. The proposed antenna system is composed of two types of antenna modules. One is multi-band module which is composed of two identical antenna elements (Ant-1 and Ant-2). This module covers 2G,

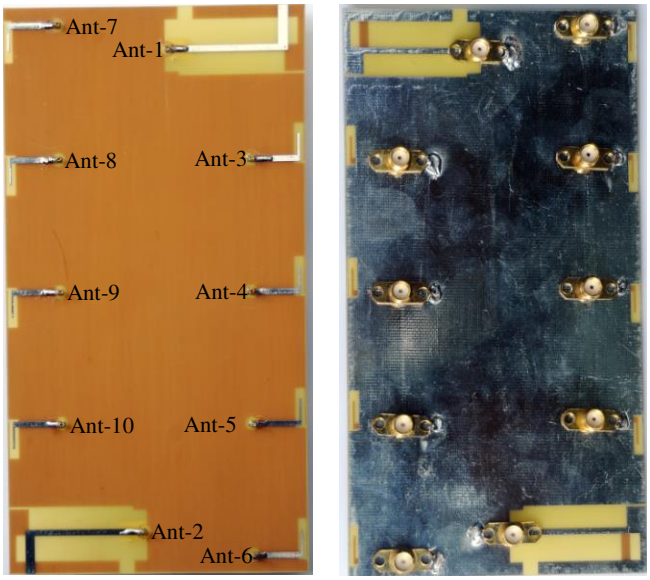

(a) (b)

FIGURE 2: Pictures of the fabricated prototypes. (a) Front view. (b) Back view.

3G, and 4G bands for mobile communication. The second module comprised of eight identical antenna elements (Ant-3 to Ant-10) covers the C- band for 5G applications. Typical simulation and measured results such as S-parameters, ECCs, surface current distributions, radiation efficiencies, antenna gains, radiation patterns, and channel capacity are calculated and presented.

II. ANTENNA DESIGN

The geometry of the proposed antenna system is shown in Fig. 1. The proposed antenna system was printed on a conductor backed by a 0.6 mm thicker FR4 substrate with the relative permittivity of 4.3. The proposed antenna system is composed of two modules i.e., the multi-band module and the single-band module. The multi-band module contains two identical multi-band antenna elements (Ant-1 and Ant-2 shown in Fig. 1) printed on the top-right and bottom-left corners of the substrate. The single-band module is composed of eight identical single antenna elements (Ant-3 through Ant-10 as displayed in Fig. 1). The overall dimensions of the proposed antenna system are $150 \times 80 \times 0.6\ mm^3$.

A. MULTI-BAND MODULE

In the multi-band module, each antenna element consists of two metallic layers, i.e., the L-shaped metallic strip printed on the FR4 substrate, and the U-shaped metallic strip etched in the ground-plane. The L-shaped strip acts as a feeder, while the U-shaped strip acts as a radiator. As shown in Fig. 1(c), the overall size of each element of the multi-band antenna is 36.9 mm $\times$ 18 mm. Each antenna element covers the six bands of modern mobile communication, i.e., GSM 850/900, GSP 1575, DCS 1800, PCS 1900, UMTS 2100, and LTE 2300/2500.

B. SINGLE-BAND MODULE

In the single-band module, eight identical antenna elements are printed along the two long side of the substrate, with an inter-element spacing of 0.41 λ = 35 mm (λ is the wavelength at f = 3.5 GHz). Each antenna element consists of a rectangular slot and L-shaped metallic strip. The rectangular slot which acts as a radiator was etched in the ground-plane with a tiny slit in the outer edge of the slot for impedance matching. The L-shaped metallic strip was printed on the top layer of the FR4 substrate. The L-shape strip contains the 50 Ω vertical feeding strip, and the horizontal strip responsible for tuning. By adjusting the width and length of the horizontal strip, the antenna elements can be tuned to the desired frequency bands.

III. RESULTS AND DISCUSSION

The proposed antenna system is fabricated and tested. Fig. 2 portrays the top and bottom views of the fabricated prototype.

A. S-PARAMETERS

The simulated and measured S-parameters (reflection and transmission coefficients) of the multi-band module (Ant-1 and Ant-2) are shown in Figs. 3(a) and (b), respectively. With a -6 dB reflection coefficient threshold [32]–[34], three resonances are observed at 900 MHz, 2 GHz, and 2.4 GHz with corresponding bandwidths of 17 % (817-970 MHz), 23 % (1.52-29.04 GHz) and 26 % (2.04-2.69 GHz), respectively. These frequency bands cover the GSM 850/900/1800/1900 MHz, GPS 1575 MHz, UMTS 2100 MHz, and LTE 2300/2500 MHz bands. Additionally, the multi-band module exhibits high isolation level (well below -12 dB) over the achieved bandwidths, as shown in Fig. 3(b).

Figs. 3(c) and (d) show the simulated and measured reflection and transmission coefficients of the single-band module. Owing to the symmetrical arrangements of the elements on the left and right sides of the substrate, and same reflection, and transmission characteristics, only the results of Ant-3 to Ant-6 (right side of the array) are displayed in Figs. 3. Antenna elements on the left side of the substrate (Ant-7 to Ant-10) are mirror images of those on the right side of the substrate, and hence, have the same reflection and transmission characteristics. It is clearly shown in Fig. 3(c) that the reflection coefficients [S_{ii}], (i = 3-6) in the single-band module are lower than -10 dB over the 3.3-3.8 GHz band. Furthermore, Fig. 3(d) shows that the transmission coefficients between any two adjacent elements, for example, the transmission coefficients between the vertical adjacent elements such as Ant-3 and Ant-4 or Ant-4 and Ant-5 are lower than -10 dB. It is noteworthy that the transmission coefficients between the horizontal nearby opposite side antennas, for example, Ant-3 and Ant-8 or Ant-4 and Ant-9 are lower than -20 dB over the desired frequency band. A good agreement between the simulated and measured results

This article has been accepted for publication in a future issue of this journal, but has not been fully edited. Content may change prior to final publication. Citation information: DOI 10.1109/ACCESS.2020.3042750, IEEE Access

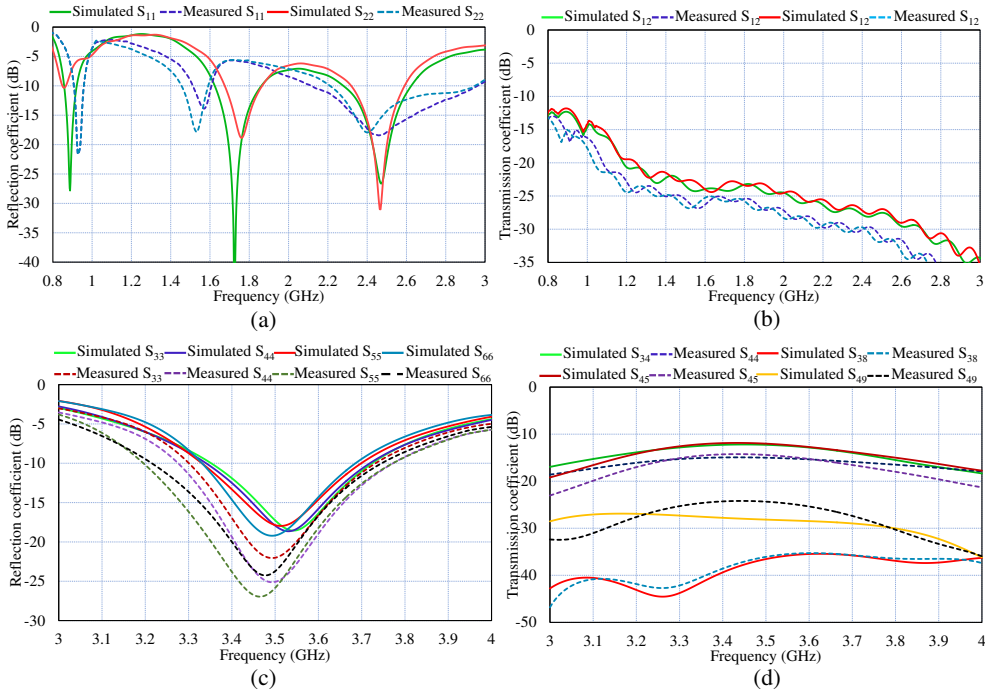

FIGURE 3: Simulated and Measured S-Parameters. (a) Reflection coefficients of the multi-band antennas. (b) Transmission coefficients of the multi-band antenna elements. (c) Reflection coefficients of the single-band antenna elements. (d) Transmission coefficients of the single-band antenna elements.

can be observed in Fig. 3. The small discrepancies between the simulated and measured results may be attributed to the soldering of the SMA connectors and fabrication tolerances.

B. PARAMETRIC STUDIES

As shown in the Fig. 3(a) each antenna element in the multiband antenna module display three resonance modes, in this parametric studies these three resonance modes will be referred to as (1) lower frequency band, (2) middle frequency band and (3) higher frequency band. Firstly, the three resonance modes randomly tuned by appropriately selecting the dimensions of L_1 , L_2 and W_1 parameters. To study the effects of the length of L_1, the length of L_1 is slightly alter from 28.4 mm to 34.4 mm, as shown in Fig. 4 (a) by increasing the length of L_1 the middle and higher frequency bands shifts to the left (lower frequency bands) while the lower frequency band remain almost fixed, For lower frequency band the resonance quarter-wavelength corresponding to L_4, L_2 and L_1, which is much longer length as compared to L_1 length, therefore L_1 has less effects on the lower frequency band as compared to higher frequency band. Fig. 4 (b) shows the effects of L_2 on the reflection coefficient, as the shown by changing L_2 from 15 mm to 17 mm the lower and higher frequency bands are alter , while the middle frequency band remain same. For the higher frequency band the width of the slot is decreasing by increasing the width of W_1, which narrow the the width of the slot and shorten the current path. Therefore the higher frequency band shifts to the higher frequency band. In short the W_1 may be used to tune the multiband antenna elements at desired frequency bands.

The parametric studies of the 5G antenna module has been also carried out. The effects of various length and width (including L_5, L_6 and W_3) has studied and analyzed. Fig. 4 (d) display the effects of narrow matching strip (L_5) on the resonances frequency. When the length of the strip increased from 10 mm to 10.30 mm the resonance frequency shifts to lower frequencies from 3.56 GHz to 3.37 GHz. The resonance frequency also effected by the width of the slot (W_3), as illustrate in the Fig. 4 (e) the resonance frequency tuned to higher frequency band by increasing the slot width from 2 to 2.5 mm the operational frequency shifts from 3.5 to 3.7 GHz. Fig. 14(f) shows that L_6 is another parameter which effects the resonance frequency, the length of L_6 is increased from 4.3 to 5.3 GHz the resonance shifts to lower frequency from 3.57 to 3.5 GHz.

C. ENVELOP CORRELATION COEFFICIENT (ECC)

Envelop correlation coefficient (ECC) is one of the key parameters in MIMO applications. ECC is used to calculate the diversity gain and channel capacity in MIMO systems. Mathematically, ECC can be calculated from the S-parameters, as well as from 3D radiation patterns. The S-parameter method is simple and fast but less accurate, while the radiation pattern method is more accurate but time consuming and complicated. In this work, the S-parameters technique is used

This article has been accepted for publication in a future issue of this journal, but has not been fully edited. Content may change prior to final publication. Citation information: DOI 10.1109/ACCESS.2020.3042750, IEEE Access

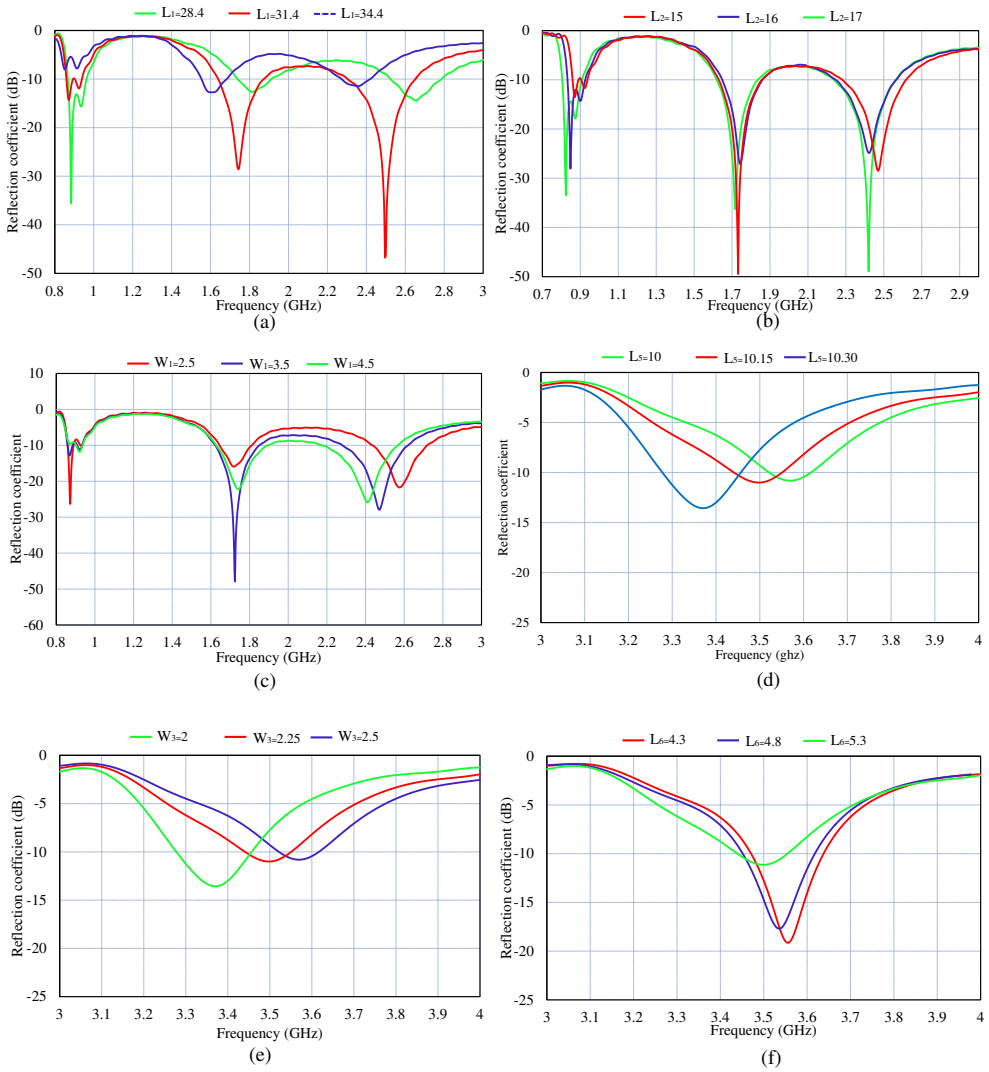

FIGURE 4: Simulation reflection coefficients of the multiband and single band antenna module as function of different lengths and widths (a) L_1. (b) L_2. (c) W_1.(d) L_5 (e) W_3 (f) L_6.

to calculate the ECC of the proposed antenna system [35].

$$ECC = \frac{|S_{ii} * S_{ij} + S_{ji} * S_{jj}|^2}{(1 - |S_{ii}|^2 - |S_{ji}|^2(1 - |S_{jj}|^2 - |S_{ji}|^2))} \quad (1)$$

The simulated and measured ECC of the multi-band and single-band antenna modules are found in close agreement which are illustrated in Fig. 5(a) and (b), respectively. The envelope correlation coefficient lies within the expected range, with a value of ECC <0.3 for multi-band antenna module and ECC <0.1 for the single band module.

D. RADIATION EFFICIENCY AND ANTENNA PEAK GAIN

Figs. 6(a) and (b) depict the simulated and measured radiation efficiencies for the multi-band and single-band antenna elements, respectively. As obvious, the radiation efficiency of multi-band elements ranges between 75 % and 90 %, while the radiation efficiency of single-band elements ranges between 60 % and 85 %. The simulated and measured peak gains for the multi-band and single-band antenna elements are plotted against the frequency in Figs. 6(c) and (d), respectively, along the boresight direction. The single element antenna gain in the multi-band module ranges between 2.1 dBi to 4 dBi. Similarly, in the single-band module, the peak gain of the antenna ranges between 2 dBi to 3.5 dBi over the targeted bandwidth. As the frequency increases, the effective aperture of the single antenna element increases, and hence its peak gain increases.

E. CURRENT DISTRIBUTION

In order to further investigate the operational mechanism of the proposed antenna system, the simulated surface current distributions at different frequencies (900 MHz, 1800 MHz, 1900 MHz, 2100 MHz, and 2500 MHz (multi-band module) and 3.5 GHz (single-band module)) are demonstrated in Fig. 7. The multi-band antenna element consists of L-shaped feeding strip and U-shaped radiating strip. The L-shaped

This article has been accepted for publication in a future issue of this journal, but has not been fully edited. Content may change prior to final publication. Citation information: DOI 10.1109/ACCESS.2020.3042750, IEEE Access

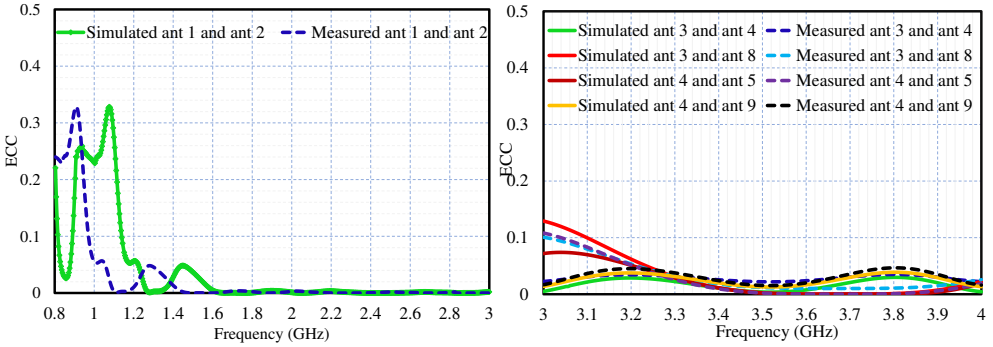

FIGURE 5: Simulated and measured Envelop correlation coefficients (ECC) of the proposed MIMO system. (a) multiband antenna module. (b) single band antenna module.

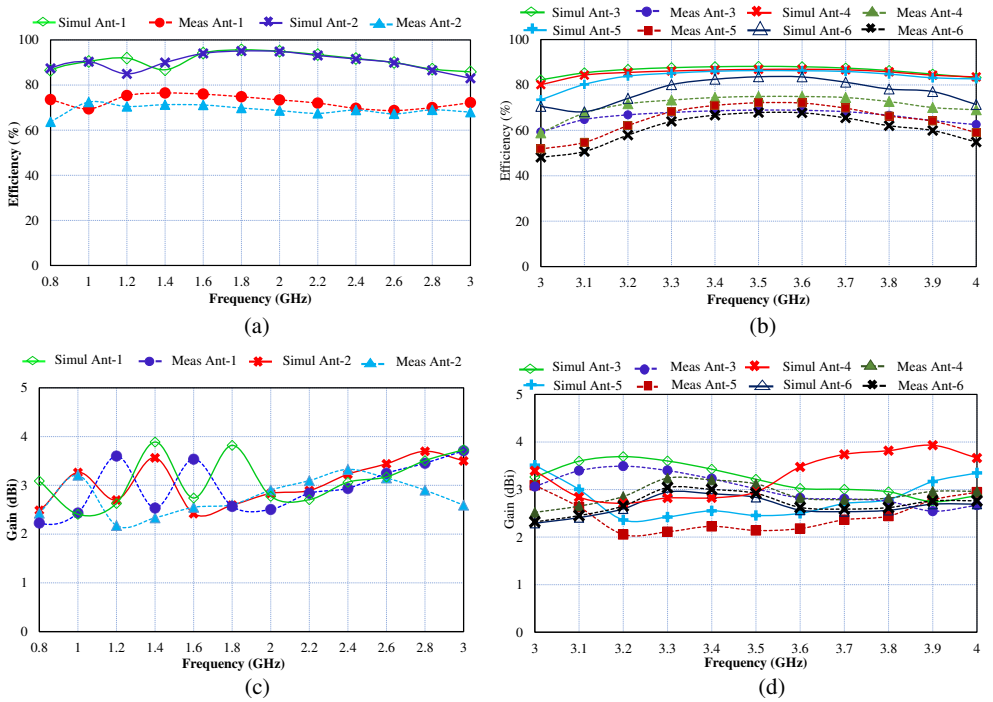

FIGURE 6: Simulated and measured radiation efficiency and antenna Gain. (a) Radiation efficiencies of multi-band antenna elements. (b) Radiation efficiencies of the singe-band antenna elements. (c) Antenna gains of multiband antennas elements. (d) Antenna Gains of single band antenna elements.

feeding strip effectively couples the energy to the U-shaped radiating strip, which produces multiple resonance modes. These resonance modes cover most of the bands for modern mobile communications. The bottom U-shaped radiating strip acts as a quarter wavelength ($\lambda/4$) monopole. As can be seen in Fig. 7(a) for lower frequency bands, the surface current covers the entire U-shaped stub. Similarly, for the middle and high frequency bands, surface current cover some portion of the U-shaped radiating stub. Fig. 7(d) represents the surface current distribution of Ant-3 (representing all other 5G antenna elements) at 3.5 GHz. Strong currents can be found on the open end of the slot, while weak currents are present on the closed end and away from the slot. This leads to low mutual coupling (high isolation) between adjacent antenna elements.

F. RADIATION PATTERNS

In this section, the simulated and measured 2D radiation patterns (E-plane and H-plane) of the multi-band and single-band antenna elements are presented and discussed. As in the multi-band module, Ant-1 and Ant-2 are identical; therefore, only for the Ant-1, the radiation patterns are displayed at 900 MHz, 1700 MHz, and 2500 MHz in Fig. 8 (a)-(c). As evident from Fig. 8(a), at lower frequency bands, the maximum radiation occurs along the boresight directions (0^o and 180^o), and minimum power is radiated along the substrate edges

Ref.	Impedance Bandwidth (GHz)	Isolation (dB)	ECC	Efficiency (%)	Single Antenna Element Size (mm^3)	Channel Capacity (bps/Hz)
[7]	3.4–3.6 (–10 dB)	> 10	< 0.2	62-78	16.7×3×0.8	39 (8 × 8, 20-dB SNR)
[36]	3.4-3.6 (–6 dB)	>10	<0.15	40-52	10×1×3.19	35 (8 × 8, 20-dB SNR)
[37]	3.4-3.6 (–10 dB)	> 12	<0.1	50–56	Not mentioned	38.8 (8 × 8, 20-dB SNR)
[38]	2.55–2.65 (–10 dB)	>12	<0.15	48-63	17.8 × 4 × 1	40(8 × 8, 20-dB SNR)
[39]	2.54–2.62 (–10 dB)	>10	<0.1	52-70	15 × 14 × 1	Not Mentioned
This work	3.4 – 3.6 (-10 dB)	> 12	<0.02	60-90	10 × 3 × 0.6	42 (8 × 8, 20-dB SNR)

TABLE 3: Proposed 5G antenna performance comparison with recent studies.

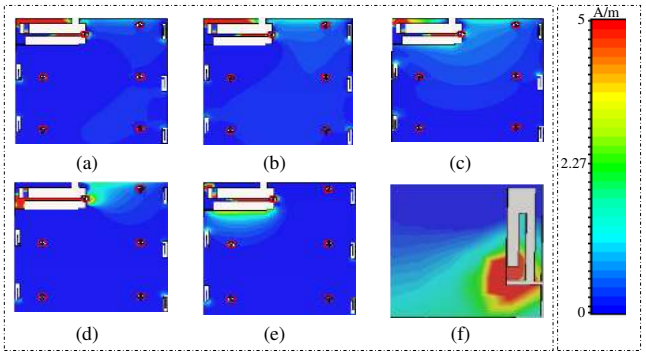

FIGURE 7: Simulated surface current distribution. (a) Ant-1 at 900 MHz. (b) Ant-1 at 1800 MHz. (c) Ant-1 at 1900 MHz. (d) Ant-1 at 2100 MHz. (e) Ant-1 at 2500 MHz. (f) Ant-3 at 3500 MHz (representing all other 5G antenna elements).

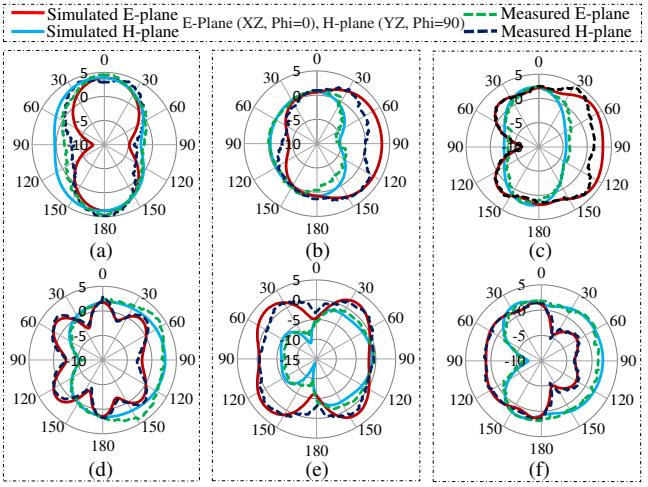

FIGURE 8: Simulated and measured 2D radiation pattern of the proposed MIMO system. (a) Ant-1 at 900 MHz. (b) Ant-1 at 1700 MHz. (c) Ant-1 at 2500 MHz. (d) Ant-3 at 3500 MHz. (e) Ant-4 at 3500 MHz. (f) Ant-5 at 3500 MHz.

(90^o and 270^o directions). Similarly, as can be seen in Figs. 8(b) and (c), at high frequency , the maximum radiation is observed in the 90^o directions.

Figs. 8(d)-(f) show the radiation patterns of Ant-3 to Ant 5 in the single-band module at 3500 MHz. As already mentioned, the right side array (Ant-3 to Ant-6) are the mirror images of the left side array (Ant-7 to Ant-10). Therefore, the radiation patterns of the right-side array are distinct complementary of the left-side, because the orientation of the antenna elements of the right side array is opposite to the left side array (180^o opposite to each other). These characteristics are advantageous for achieving low ECC in the desired frequency bands.

G. CHANNEL CAPACITY

The channel capacity in a typical MIMO communication system can be calculated using the mathematical formula given below [36].

$$C = Nlog_2(1 + \frac{\rho}{n})(1 - r_{ij}) \quad (2)$$

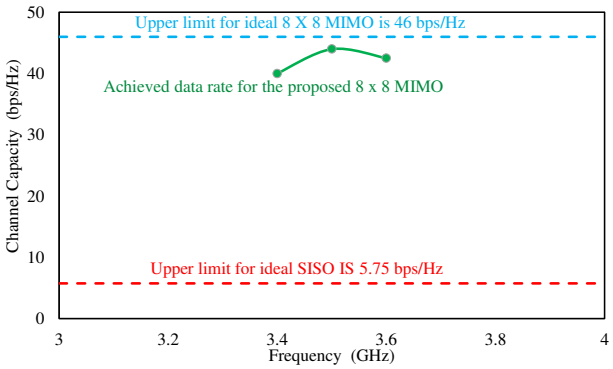

FIGURE 9: Calculated channel capacity of the proposed MIMO antenna system.

where N is the number of antennas, ρ is the signal power, n is

This article has been accepted for publication in a future issue of this journal, but has not been fully edited. Content may change prior to final publication. Citation information: DOI 10.1109/ACCESS.2020.3042750, IEEE Access

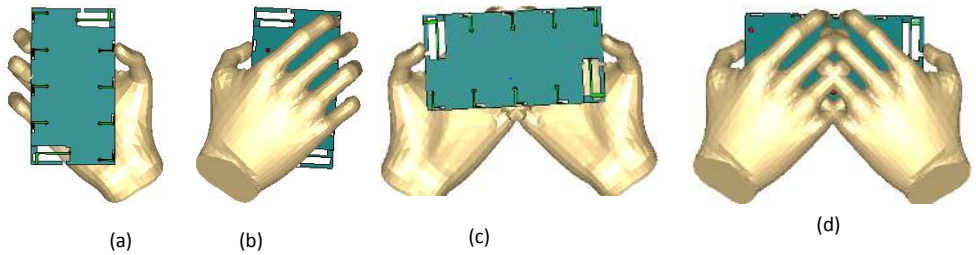

FIGURE 10: Different usage postures of SHM and DHM. (a) front view of SHM. (b) back view of SHM. (c) front view of DHM. (d) back view of DHM.

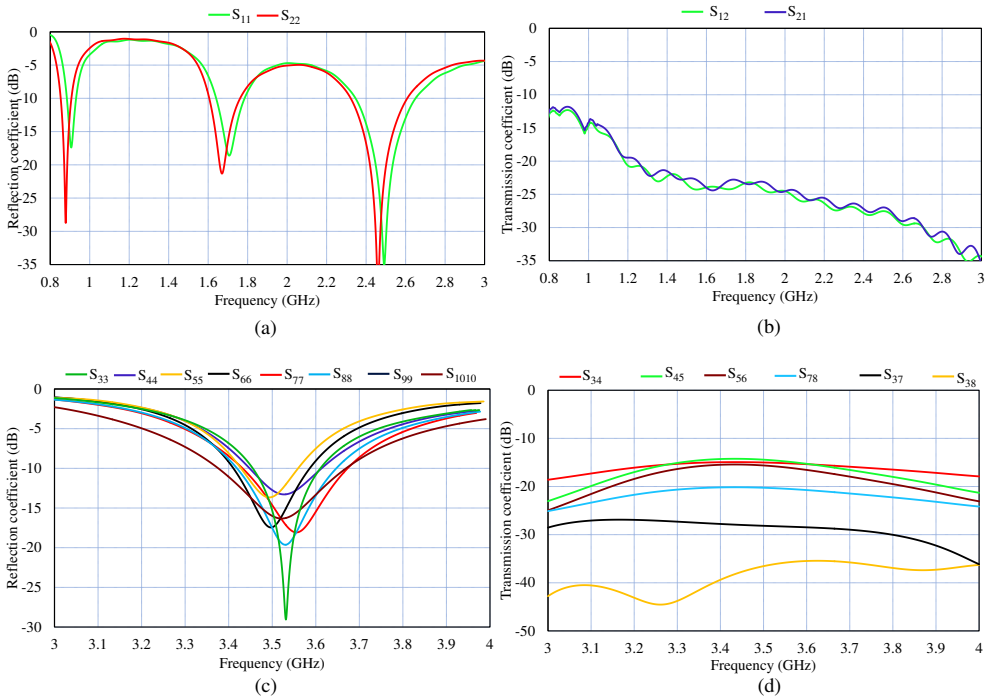

FIGURE 11: Simulation S-parameters results of the SHM operation (a) reflection coefficients of multiband antenna module (b) transmission coefficients of multiband antenna module (c) Reflection coefficient of single band antenna module (d) transmission coefficients of single antenna module.

the noise power, and *r* is the envelop correlation coefficient between i^{th} and j^{th} antenna elements.

In this case, the channel capacity for 5G antenna elements (single-band module) was calculated by assuming that the transmitting antenna elements are uncorrelated. Furthermore, the channels between transmitting and receiving antennas were supposed to be independent and identically distributed (i.i.d) with Raleigh fading environment and 20 dB signal-to-noise ratio (SNR). The simulated channel capacity plots for the proposed antenna system are depicted in Fig. 9. For comparison purposes, the ideal channel capacity of a single-input-single-output (SISO) and 8 $\times$ 8 MIMO systems are added. The calculated channel capacity of the proposed single-band module elements is 43 bps/Hz over the 3.5 GHz bandwidth.

H. USER'S HANDS EFFECTS

In order to investigate and study, the user's hand effects on the the performance of the proposed antenna system. The two typical usage scenarios, the single-hand mode (SHM) and double-hand mode(DHM) scenario are presented and discussed in this section. The two different usage postures of SHM and DHM are shown in the Fig. 10. some typical simulation results, such as reflection coefficients, transmission coefficients, envelop correlation coefficients and antenna efficiencies in the SHM (talking mode) and DHM (data mode) are presented.

The simulation results of the SHM operations is shown in the in Figs. 11 and 12, as shown in the Figs. 13 (a) and (b) the reflection coefficients of the multiband and single band antenna module are not significantly effected by user's hand. However, the impedance matching of the some the antenna elements, which is directly touch or closed to figures (ant

This article has been accepted for publication in a future issue of this journal, but has not been fully edited. Content may change prior to final publication. Citation information: DOI 10.1109/ACCESS.2020.3042750, IEEE Access

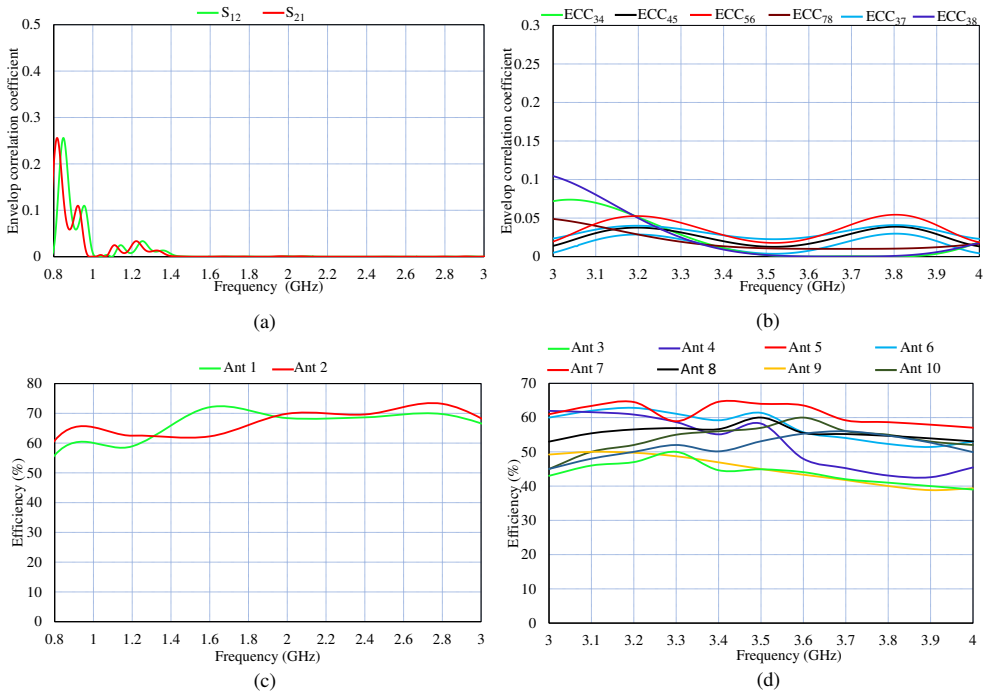

FIGURE 12: Simulation ECC and antenna efficiencies of the SHM operation (a) envelop correlation coefficient of the multiband antenna module (b) envelop correlation coefficient of single band antenna module. (c) antenna efficiencies of multiband antenna module (d) antenna efficiencies of single band antenna module.

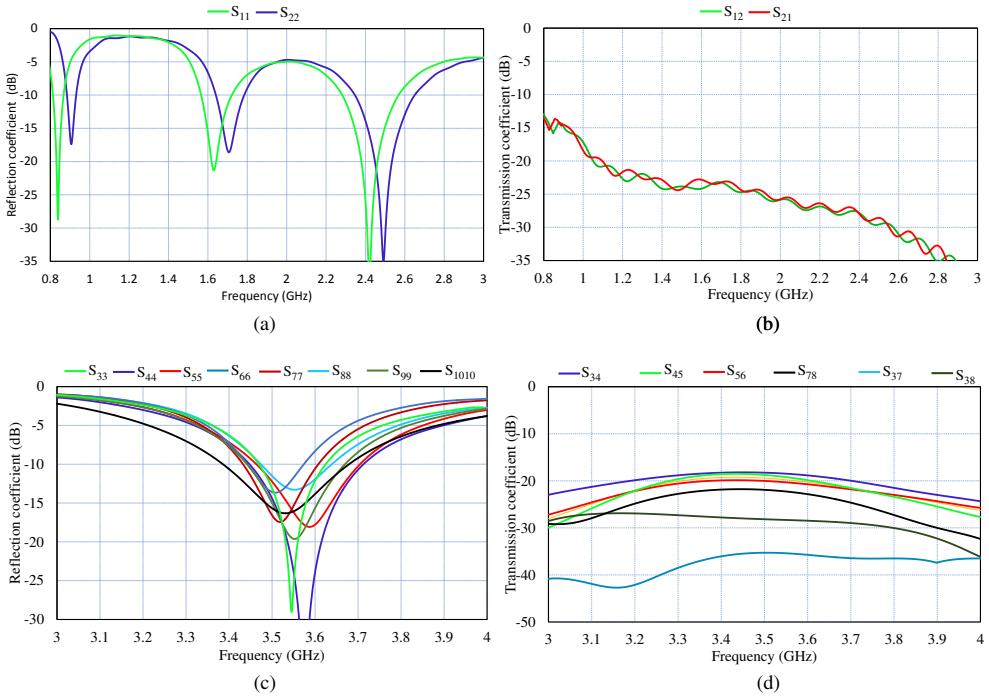

FIGURE 13: Simulation S-parameters results of the DHM operation (a) reflection coefficients of multiband antenna module (b) transmission coefficients of multiband antenna module (c) Reflection coefficient of single band antenna module (d) transmission coefficients of single antenna module.

3, ant 7 and ant 8) are slightly shifted to higher frequency bands, but could still cover the desired frequency bands. The isolation between antenna elements increases due to energy absorption by user hand, while the envelop correla-

This article has been accepted for publication in a future issue of this journal, but has not been fully edited. Content may change prior to final publication. Citation information: DOI 10.1109/ACCESS.2020.3042750, IEEE Access

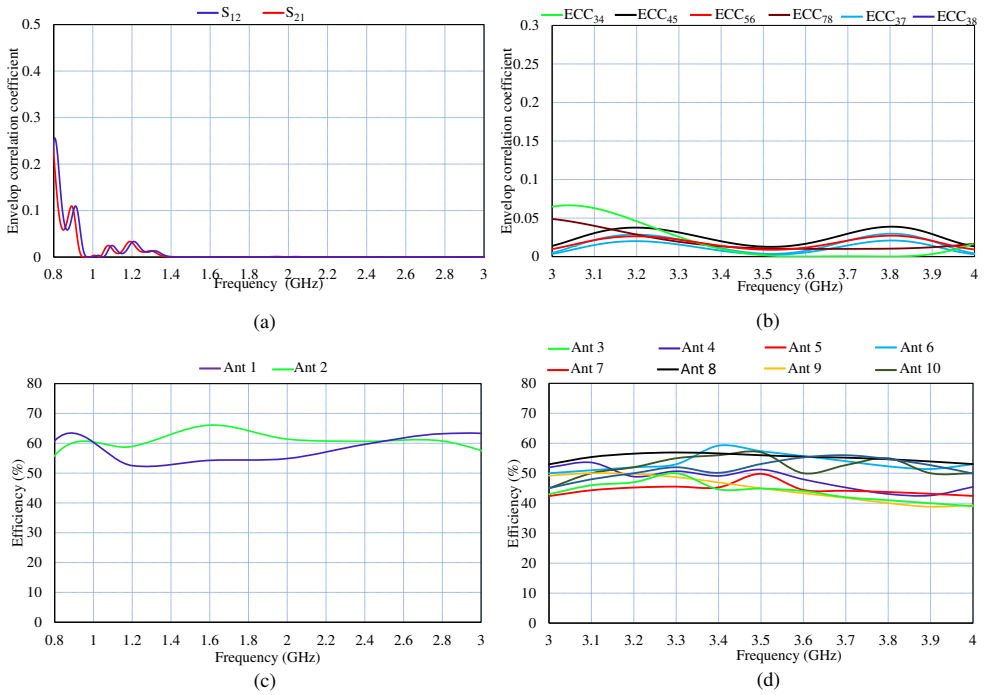

FIGURE 14: Simulation ECC and antenna efficiencies of DHM operation (a) envelop correlation coefficient of the multiband antenna module (b) envelop correlation coefficient of single band antenna module. (c) antenna efficiencies of multiband antenna module (d) antenna efficiencies of single band antenna module.

tion coefficients are not significantly effected by user hand and remain almost same, as shown in the Figs. 12 (a) and (b). furthermore, the antenna efficiencies of the multiband and single band antenna elements are significantly effected by user's hand, due to electromagnetic energy absorptions by user's hand. It is shown in Figs. 12 (c) and (d) the efficiencies of the multiband antenna elements are reduced approximately 19 %, which the efficiencies of some of the antenna elements (ant 3, ant 7 and ant 8) in single band antenna module are declined approximately 32 %, because these antenna elements are directly touch or very closed to user's hand. A similar results can be observed in the Figs. 13 and 14 for the DHM operation, as shown in figures the reflection coefficients, transmission coefficients and envelop correlation coefficients are less effected by user's hands, while the antenna efficiencies are significantly effected by user's hands.

I. PERFORMANCE COMPARISON

Table 3 shows the detailed comparison of the proposed work with some of the latest works reported in literature. This comparison is based on isolation, ECC, radiation efficiency, number of antenna elements, size of individual antenna elements, and channel capacity. The individual element size of our proposed antenna system is $10 \times 3\ mm^2$ which is smallest compared to [37], [39], [40], and the multi-mode MIMO system reported in [7]. Considering the ECC, our proposed antenna has better ECC compared to [7], [37], and [39], while it is comparable with [38] and [39]. Furthermore, the isolation (mutual coupling) of the recommended MIMO antenna system is lower compared to those listed in Table 3. The radiation efficiency and channel capacity of our design are also better among all antennas listed in Table 3. Moreover, the proposed MIMO system is one of the few MIMO antenna system that covers 2G, 3G, 4G, and 5G bands, whereas all the reported MIMO system listed in table (except [7]) are single mode, thus can be applicable only for 5G bands.

IV. CONCLUSION

In this paper, a 10-ports hybrid MIMO antenna system was introduced for 5G smart-phone applications. The proposed MIMO antenna system was composed of a multi-band and single-band antenna modules. Each antenna element in the multi-band module encompassed 2G, 3G, and 4G bands, while the single-band module composed of eight identical monopole antenna elements covered the C-band for 5G applications. The peak channel capacity of 43 bps/Hz was achieved for the proposed MIMO antenna system. The comparison of the typical performance parameters of the proposed antenna with those of the recently reported studies confirmed that our antenna system can be used beneficially in the modern smart-phones.

V. ACKNOWLEDGMENTS

The publication of this article was funded by the Abu-Dhabi Department of Education and Knowledge (ADEK) Award for Research Excellence, in 2019, under Grant AARE19-245.

REFERENCES

[1] M. Z. Chowdhury, M. Shahjalal, S. Ahmed, and Y. M. Jang,"6G wireless communication systems: applications, requirements, technologies, challenges, and research directions," *IEEE Open Journal of the Communications Society,* vol. 1, pp. 957–975, 2020.

[2] T. Huang, W. Yang, J. Wu, J. Ma, X. Zhang, and D. Zhang, "A survey on green 6G network: architecture and technologies," *IEEE Access,* vol. 7, pp. 175758–175768, 2019.

[3] M. Abdullah, S. H. Kiani, and A. Iqbal, "Eight element multiple-input multiple-output (MIMO) antenna for 5G mobile applications," *IEEE Access,* vol. 7, pp. 134488–134495, 2019.

[4] Z. Xu and C. Deng, "High-isolated MIMO antenna design based on pattern diversity for 5G mobile terminals," *IEEE Antennas and Wireless Propagation Letters,* vol. 19, no. 3, pp. 467–471, March. 2020.

[5] K. Shafique, B. A. Khawaja, F. Sabir, S. Qazi, and M. Mustaqim, "Internet of things (IoT) for next-generation smart systems: a review of current challenges, future trends and prospects for emerging 5G-IoT scenarios," *IEEE Access,* vol. 8, pp. 23022–23040, 2020.

[6] J. Choi, W. Hwang, C. You, B. Jung, and W. Hong, "Four-element reconïňĄgurable coupled loop MIMO antenna featuring LTE full-band operation for metallic-rimmed smartphone," *IEEE Transactions on Antennas and Propagation,* vol. 67, no. 1, pp. 99–107, Jan. 2019.

[7] Y. Li, C. Li, C. Sim, G. Wu and k. Wong, "4G/5G Multiple Antennas for Future Multi-Mode Smartphone Applications, "*IEEE access,* vol. 4, pp. 2981–2988, July. 2016.

[8] WRC-15 Press Release. (Nov. 27, 2015). World Radiocommunication Conference Allocates Spectrum for Future Innovation. [Online]. Available: http://www.itu.int/net/pressof-ce/press-releases/2015/56.aspx. Retrieved on 2019.

[9] M. M. Blue, S. Yrjola, V. seppanen, P. Ahokangas, H. Hammainen, and M. L. Aho, "Analysis of spectrum valuation elements for local 5G networks: case study of 3.5 GHz band," *IEEE Transactions on Cognitive Communications and Networking,* vol. 5, no. 3, pp. 741–753, Sept. 2019.

[10] E. Lagunas, C. G. Tsinos, S. K. Sharma, and S. Chatzinotas, "5G cellular and fixed satellite service spectrum coexistence in C-band," *IEEE Access,* vol. 8, pp. 72078–72094, 2020.

[11] N. Hussain, M. Jeong, A. Abbas, T. Kim, and N. Kim, "A metasurface-based low-profile wideband circularly polarized patch antenna for 5G millimeter-wave systems," *IEEE Access,* vol. 8, pp. 22127–22135, 2020.

[12] N. K. Sahu, G. Das, and R. K. Gangwar, "Dielectric resonator based MIMO antenna with circular polarization diversity for WiMAX applications," *PhotonIcs & Electromagnetics Research Symposium - Spring (PIERS-Spring), Rome, Italy,* pp. 604–612, 2019.

[13] Dioum, A. Diallo, S. M. Farssi, and C. Luxey, "A novel compact dual-band LTE antenna-system for MIMO operation," *IEEE Transactions on Antennas and Propagation,* vol. 62, no. 4, pp. 2291–2296, April. 2014.

[14] W. Han, X. Zhou, J. Ouyang, Y. Li, R. Long, and F. Yang, "A six-port MIMO antenna system with high isolation for 5-GHz WLAN access points," *IEEE Antennas and Wireless Propagation Letters,* vol. 13, pp. 880–883, 2014.

[15] J. Deng, J. Li, L. Zhao, and L. Guo, "A dual-band inverted-F MIMO antenna with enhanced isolation for WLAN applications," *IEEE Antennas and Wireless Propagation Letters,* vol. 16, pp. 2270–2273, 2017.

[16] Y. Ding, Z. Du, K. Gong, and Z. Feng, "A novel dual-band printed diversity antenna for mobile terminals," *IEEE Transactions on Antennas and Propagation,* vol. 55, no. 7, pp. 2088–2096, July. 2007.

[17] S. Khan, H. Ali, R. Khan, R. Harry, and C. Tanougast, "A cross-shaped MIMO reconfigurable dielectric resonator antenna for GSM and LTE/UMTS applications," *29th Irish Signals and Systems Conference (ISSC), Belfast,* pp. 1–4, 2018.

[18] L. Alex and S. Amma, "Compact inverted U shaped slot triple band MIMO antenna for WLAN and WiMAX applications," *Second International Conference on Inventive Communication and Computational Technologies (ICICCT), Coimbatore,* pp. 1034–1036, 2018.

[19] C. F. Ding, X. Y. Zhang, C. D. Xue, and C. Y. D. Sim, "Novel pattern diversity-based decoupling method and its application to multielement MIMO antenna," *IEEE Transactions on Antennas and Propagation,* vol. 66, no. 10, pp. 4976–4985, Oct. 2018.

[20] L. Chang, Y. Yu, K. Wei, and H. Wang, "Orthogonally-polarized dual antenna pair with high isolation and balanced high performance for 5G MIMO smartphone," *IEEE Transactions on Antennas and Propagation, early access,* Jan. 9, 2020.

[21] L. Sun, Y. Li, Z. Zhang, and Z. Feng, "Wideband 5G MIMO antenna with integrated orthogonal-mode dual-antenna pairs for metal-rimmed smartphones," *IEEE Transactions on Antennas and Propagation,* vol. 68, no. 4, pp. 2494–2503, April. 2020.

[22] W. Jiang, B. Liu, Y. Cui, and W. Hu, "High-isolation eight-element MIMO array for 5G smartphone applications," *IEEE Access,* vol. 7, pp. 34104–34112, 2019.

[23] W. Hu, L. Qian, S. Gao, L. H. Wen, Q. Luo, H. Xu, X. Liu, Y. Liu, and W. Wang, "Dual-band eight-element MIMO array using multislot decoupling technique for 5G terminals," *IEEE Access,* vol. 7, pp. 153910–153920, 2019.

[24] X. Zhang, Y. Li, W. Wang, and W. Shen, "Ultra-wideband 8-Port MIMO antenna array for 5G metal-frame smartphones," *IEEE Access,* vol. 7, pp. 72273–72282, 2019

[25] R. Ullah, S. Ullah, B. Kamal, and R. Ullah, "A four-port multiple input multiple output (MIMO) antenna for future 5G smartphone applications," *International Conference on Electrical, Communication, and Computer Engineering (ICECCE), Swat, Pakistan,* pp. 1–5, 2019.

[26] Z. Ren and A. Zhao, "Dual-band MIMO antenna with compact self decoupled antenna pairs for 5G mobile applications," *IEEEAccess,* vol.7, pp. 82288–82296, 2019.

[27] J. Li, X. Zhang, Z. Wang, X. Chen, J. Chen, Y. Li, and A. Zhang, "Dual-band eight-antenna array design for MIMO applications in 5G mobile terminals," *IEEE Access,* vol. 7, pp. 71636–71644, 2019.

[28] J. Park, M. Rahman, and H. N. Chen,"Isolation enhancement of wide-band MIMO array antennas utilizing resistive loading," *IEEE Access,* vol. 7, pp. 81020–81026, 2019.

[29] Y. Li, C. Sim, Y. Luo, and G. Yang, "Multiband 10-antenna array for sub-6 GHz MIMO applicationsin 5-G smartphones," *IEEEAccess,* vol.6, pp. 28041–28053, 2018.

[30] Y. Li, C. Sim, Y. Luo, and G. Yang, "12-Port 5G massive MIMO antenna array in sub-6GHz mobile handset for LTE bands 42/43/46 applications," *IEEE Access,* vol. 6, pp. 344–354, 2018.

[31] Y. Liu, A. Ren, H. Liu, H. Wang, and C.-Y.-D. Sim, "Eight-port MIMO array using characteristic mode theory for 5G smartphone applications," *IEEE Access,* vol. 7, pp. 45679–45692, 2019.

[32] R. Hussain, A. T. Alreshaid, S. K. Podilchak, and M. S. Sharawi, "Compact 4G MIMO antenna integrated with a 5G array for current and future mobile handsets," *IET Microwaves, Antennas & Propagation,* vol. 11, no. 2, pp. 271–279, 2017.

[33] Z. Xu, Q. Zhou, Y. Ban, and S. S. Ang, "Hepta-band coupled-fed loop antenna for LTE/WWAN unbroken metal-rimmed smartphone applications," *IEEE Antennas and Wireless Propagation Letters,* vol. 17, no. 2, pp. 311–314, Feb. 2018.

[34] A. Biswas and V. R. Gupta, "Design of penta-band MIMO antenna for GPS/2G/3G/4G and 5G NR applications," *International Journal of Recent Technology and Engineering (IJRTE),* vol. 8, pp. 1935–1940, May. 2019.

[35] M. S. Sharawi, "Printed multi-band MIMO antenna systems and their performance metrics [Wireless Corner]," *IEEE Antennas and Propagation Magazine,* vol. 55, no. 5, pp. 218–232, Oct. 2013.

[36] G.Srinivasarao, "Algorithm approach to multiple input multiple output (MIMO) systems," *International Journal of Innovative Research in Computer and Communication Engineering,* vol.3, no.2, pp. 11918–11924, Nov. 2015.

[37] K. Wong, C. Tsai and J. Lu, "Two asymmetrically mirrored gap-coupled loop antennas as a compact building block for eight-antenna MIMO array in the future smartphone," *IEEE Transactions on Antennas and Propagation,* vol. 65, no. 4, pp. 1765–1778, April. 2017.

[38] H. Zou, Y. Li, C. Y. D. Sim, and G. Yang. "Design of 8 $\times$ 8 dual-band MIMO antenna array for 5G smartphone applications," *International journal of RF and microwave computer AIDED Engineering,* vol. 4, pp. 1–12, May. 2018.

[39] M. Y. Li et al., "Eight-port orthogonally dual-polarized antenna array for 5G smartphone applications," *IEEE Transactions on Antennas and Propagation,* vol. 64, no. 9, pp. 3820–3830, Sep. 2016.

[40] Z. Qin, W. Geyi, M. Zhang, and J. Wang, "Printed eight-element MIMO system for compact and thin 5G mobile handset," *Electron. Lett.,* vol. 52, no. 6, pp. 416–418, Mar. 2016.

This article has been accepted for publication in a future issue of this journal, but has not been fully edited. Content may change prior to final publication. Citation information: DOI 10.1109/ACCESS.2020.3042750, IEEE Access

RIZWAN ULLAH was born in Khyber Pakhtunkwa, Pakistan, in 1993. He received his B.Sc. degree in Telecommunication Engineering from University of Engineering and Technology Peshawar, Pakistan in 2016. He obtained the M.S. degree in Telecommunication Engineering from University of Engineering and Technology, Peshawar, Pakistan. Currently, he is pursuing the Ph.D. degree in Telecommunication engineering from university of engineering and technology, Mardan, Pakistan. . His research interests mainly focuses on design and analysis MIMO antennas for 4G and 5G Smartphone, MIMO antennas for 4G/5G wireless access points, and millimeter wave array antennas for 5G communication. His research work is published in IEEE conferences.

SADIQ ULLAH is Professor and Head of Telecommunication Engineering Department, University of Engineering & Technology, Mardan, Pakistan. Sadiq Ullah received BSc electrical engineering degree from the University of Engineering and Technology, Peshawar, Pakistan. He achieved his MSc degree in electrical engineering from the University of Engineering and Technology Taxila, Pakistan. In 2007, he joined the Department of Electronic and Electrical Engineering at Loughborough University, U.K., and was awarded PhD degree for his research in the ïňĄeld of design and measurement of metamaterial-based antennas in 2010. He worked as an assistant manager (Electronics) in a public sector R and D organization in Islamabad, where his main responsibilities were hardware, software codesign, designing and testing of high precession electronics, test equipment. His research mainly focuses on design and measurement of metasurfaces, metamaterial-based antennas, 5G MIMO Antennas, multiband/wideband antenna, SAR, and wearable antennas. He has been worked as a research associate at Loughborough University, where he researched on the propagation effects of rain, snow, ice, fog, and forest in millimeter wave band. His research is published in international conferences and peer reviewed journals.
ORCID: https://orcid.org/0000-0002-5299-1577

RAZA ULLAH was born in Khyber Pakhtunkhwa, Pakistan, in 1992. He received B.Sc. degree in Telecommunication Engineering from University of Engineering and Technology, Peshawar, Pakistan in 2015. He obtained the M.S. degree in Telecommunication Engineering from University of Engineering and Technology, Peshawar, Pakistan. His research interests are designing and analyzing millimeter array antennas for 5G communications. Design MIMO antennas, for current and future 5G mobile terminals and MIMO antennas for 5G wireless access points. His research is published in IEEE conferences and peer reviewed journals.

FAROOQ FAISAL was born in Buner, Pakistan, in 1993. He received the B.Sc. degree in telecommunication engineering from University of Engineering and Technology, Peshawar, Pakistan, in 2016, and the M.Sc. degree in telecommunication engineering from University of Engineering and Technology, Taxila, Pakistan, in 2019. Currently, he is pursuing the Ph.D. degree in electrical engineering at University of Quebec, Canada. His current research interests include implantable antennas and devices, wireless power transfer, millimetre wave antennas, wearable antennas for remote underground mine monitoring systems, frequency selective surfaces, EBGs, and portable microwave hybrid imaging based scanners.

ISMAIL BEN MABROUK received the B.A.Sc. and M.A.Sc. degrees in Electrical Engineering from the University of Lille, Lille, France in 2006 and 2007, respectively, and the Ph.D. in Electrical Engineering from University of Quebec, Canada, in 2012. From 2007 to 2009 he was with Huawei Technologies, Paris, France. In 2012, he joined the Wireless Devices and Systems (WiDeS) group at University of Southern California, Los Angeles, USA. He is currently an Assistant Professor at Al Ain University, Abu Dhabi, UAE. He is a recipient of the Abu Dhabi Award for Research Excellence (AARE) âĂŞ 2018. His research activities have been centred on antenna design at the millimiter-wave and THz frequencies, propagation studies for Multiple-Input and Multiple-Output (MIMO) systems, Deep Learning, and Wireless Body Area Network for medical applications.

MUATH JODEI AL HASAN received his B.Sc. degree in electrical engineering from the Jordan University of Science and Technology, Jordan, in 2005, the M.Sc. in wireless communications from Yarmouk University, Jordan in 2008, and the Ph.D. degree in Telecommunication engineering from Institut National de la Recherche Scientifique (INRS), UniversitÃl' du QuÃl'bec, Canada, 2015. In 2013, he worked at Planet Labs. Inc, California, USA as an RF Engineer. In May 2015, he joined Concordia University as postdoctoral fellow. He is currently an Assistant Professor at Al Ain University, Abu Dhabi, UAE. Dr. Al-Hasan is the recepeint of the prestigous ADEK Award for Research Excellence in 2019. His current research interests include Millimeter-wave Antennas, Teral... bands, Channel Modling, MIMO systems, Artificial Materials.